ARTICLE

Ab initio Study on Spectral Properties of Charge-Compensated Ce^{3+} in NaF

Nai-yu Ma, Feng Yang, Xian-chun Shen, Yu-cheng Huang, Li-xin Ning*

Department of Physics, Anhui Normal University, Wuhu 241000, China

(Dated: Received on May 15, 2014; Accepted on June 24, 2014)

We report an *ab initio* study of spectral properties of Ce^{3+} doped at Na^+ site of the NaF crystal, with the charge imbalance compensated by two oxygen substitutions for fluoride (O_F') in the first coordination shell or two sodium vacancies (V_{Na}') in the second coordination sphere. Density functional theory calculations within the supercell model are first performed to optimize the local structures of the charge-compensated Ce^{3+}, based on which Ce-centered embedded clusters are constructed and wave function-based CASSCF/CASPT2/RASSI-SO calculations are carried out to obtain the energies of $4f^1$ and $5d^1$ levels. By comparing the calculated 4f→5d transition energies with experimental excitation spectra at low temperatures, the lowest 4f→5d transition band peaked at 390 nm is assigned to the Ce^{3+} with charge compensation by two coordinating O_F' substitutions, rather than to the Ce^{3+} with compensation by two V_{Na}' vacancies, as proposed earlier. The electronic reason for the large redshift (by ∼8000 cm^{-1}) of the lowest 4f→5d transition as induced by the two nearby O_F' substitutions is analyzed in terms of the changes in the centroid shift and crystal-field splitting.

Key words: *Ab initio* calculation, NaF:Ce^{3+}, Local structure, Transition

I. INTRODUCTION

Inorganic compounds activated by Ce^{3+} have received a great deal of attention for applications in scintillators [1], light-emitting diodes [2], and solid-state lasers [3], which are associated with the electric dipole-allowed 5d→4f emission of Ce^{3+} in the visible and near ultraviolet spectral region with a characteristic decay time on the order of 10^{-8} s. Available experimental data on $5d^1$ energy levels relative to the $4f^1$ ground state in a wide range of Ce-doped compounds have been compiled and analyzed, and the variation of the first $4f_1 \rightarrow 5d_1$ transition energy with crystalline environments has been rationalized in terms of centroid shift and crystal-field splitting of $5d^1$ configuration [4]. An empirical model has been developed from which, if the lowest 4f→5d transition energy of Ce^{3+} in a given host is known, the energy of the first $4f^N \rightarrow 4f^{N-1}5d$ transition of any other Ln^{3+} at the same site of the host can then be predicted with an average accuracy of ±600 cm^{-1} [5].

However, the identification of experimentally observed 4f→5d transition bands in association with local structural properties of the dopant ion is often complicated by the existence of local charge compensation. The NaF crystal doped with Ce^{3+} is such an example, where the Ce^{3+} sits on the Na^+ site and the extra positive charges may be compensated by two oxygen for fluoride substitutions (O_F', in Kröger-vink notation) or two sodium vacancies (V_{Na}'), depending on the growth or annealing condition of the crystal. Experimentally, upon excitation by UV light, the emission spectrum of NaF:Ce^{3+} crystals grown in air exhibits three bands with maxima at 472 nm (I), 517 nm (II), and 730 nm (III) at room temperature [6]. From excitation study, bands I and II have been assigned to one type of Ce^{3+} center and their separation was related to the spin-orbit splitting of the ^2F ground term (into $^2F_{5/2}$ and $^2F_{7/2}$ states), and band III to anther type. At liquid nitrogen temperature, the excitation spectrum of band I or II has two intense bands with maxima at 250 nm (40000 cm^{-1}) and 309 nm (32362 cm^{-1}), and also two weak bands with maxima at 355 nm (28169 cm^{-1}) and 390 nm (25640 cm^{-1}) [7]. Since the maxima of the former two intense bands coincide with the absorption band maxima of the crystal grown in argon atmosphere, the two intense and two weak excitation bands all together have been ascribed to the Ce^{3+} centers with two V_{Na}' as charge compensators [6, 7]. However, the redshift (by 23700 cm^{-1}) of the lowest 4f→5d transition with respect to the free ion case (49340 cm^{-1}) is too large compared with those (6000−18000 cm^{-1}) exhibited in other Ce-doped fluoride compounds. It was therefore proposed that two oxygen ions instead of two sodium vacancies could be present near the Ce^{3+} in order to account for the exceptionally large redshift [4].

*Author to whom correspondence should be addressed. E-mail: ninglx@mail.ahnu.edu.cn

 ©2014 Chinese Physical Society

To resolve this ambiguity, an *ab initio* study is expected to be helpful, since it can in principle give information on the local structure of the dopant Ce^{3+}, the 4f→5d transition energies, and also their mutual dependence [8−10]. It is worth mentioning here that NaF crystals with substitutional impurities not only are interesting as model systems for fundamental research, but also have applications as optical materials (*e.g.*, NaF:U^{6+} and NaF:Eu^{3+}) used in dosimeters of ionizing radiation [11, 12].

In the present work, we have performed first-principles calculations on Ce-doped NaF in order to elucidate experimentally observed Ce^{3+} 4f→5d transitions, especially the lowest one. Periodic DFT calculations with the supercell model were first carried out to optimize the structures of NaF:Ce^{3+} with various charge compensations. The considered types of charge compensation are two O_F' substitutions in the first coordination shell of Ce^{3+} and two V_{Na}' vacancies in the second coordination sphere. In the former case, there are two symmetrically inequivalent configurations, *i.e.*, O_{F1}'-O_{Fi}' (i=2, 3) and, in the latter case, four symmetrically inequivalent configurations exist, *i.e.* V_{Na1}'-V_{Nai}' (i=2−5) (see Fig.1). With the DFT-optimized supercell structures, Ce-centered embedded clusters were then constructed, for which the wave function-based CASSCF/CASPT2/RASSI-SO calculations were performed to obtain the energies of $4f^1$ and $5d^1$ levels with inclusion of the spin-orbit effect. By comparing the calculated 4f→5d transition energies to experiments, the experimental spectra have been interpreted, and especially the exceptionally large redshift of the lowest 4f→5d transition as described above has been addressed.

II. METHODOLOGY

To optimize the local structure of charge-compensated Ce^{3+}, the NaF:Ce^{3+} crystal was modeled by a 3×3×3 supercell (216 atoms), in which one of the 108 Na^+ ions was replaced by a Ce^{3+} with various local charge compensators. For each supercell, the lattice constants and atomic coordinates were fully optimized by DFT calculations with the GGA-PBE functional [13, 14] as implemented in the plane wave code VASP [15, 16]. The optimizations were performed using the conjugate gradient technique until the total energies were converged to 10^{-6} eV and the Hellmann-Feynman forces on the atoms were less than 0.01 eV/Å. The Na $2p^63s^1$, F $2s^22p^5$, O $2s^22p^4$, and Ce $5s^25p^64f^15d^16s^2$ electrons were treated as valence electrons and their interactions with the core were described by projector augmented wave (PAW) method [17]. A single k-point Γ was adopted to sample the Brillouin zone, and the cutoff energy for the plane wave basis was set to 550 eV.

From the DFT-optimized supercell structures, the Ce-centered embedded clusters were constructed for which the wave function-based *ab initio* calculations were performed to obtain the energies of $4f^1$ and $5d^1$ levels. Each of the embedded clusters consists of a central Ce^{3+} ion and its coordinating anions. The immediate radius 10.0 Å were described by 510−540 lattice ions modeled by AIMP embedding potentials, to account for the short-range electrostatic, exchange, and Pauli interactions of the embedded clusters with their environments. The embedding potentials for Na^+, F^-, and O^{2-} were taken from those generated for NaF [18] and $Y_3Al_5O_{12}$ [19]. The influences of the remaining crystalline environments were considered by using 69393−72871 point charges at lattice sites, as generated using Lepetit's method [20]. For these embedded clusters, the state-average CASSCF (SA-CASSCF) plus CASPT2 calculations were performed with the scalar relativistic many-electron Hamiltonian to account for the bonding, static and dynamic correlation effects. With the CASSCF wave functions and the CASPT2 energies, the AMFI approximation of the DKH spin-orbit coupling operator was added to the Hamiltonian, and a restricted active space state-interaction spin-orbit (RASSI-SO) method [21] was used to include the spin-orbit coupling effect.

In the SA-CASSCF calculations, a [4f, 5d, 6s] complete active space was adopted. No symmetry (C_1 point group) was used in the calculations, and the $4f^1$ and $5d^1$ levels are labeled by $4f_{1-7}$ and $5d_{1-5}$, respectively, in order of increasing energy. With the CASSCF wave functions and the optimized occupied and virtual molecular orbitals, CASPT2 calculations were carried out to take into account the dynamic correlation effects of the Ce^{3+} 5s, 5p, 4f, and 5d electrons and the F^- or O^{2-} 2s, 2p electrons. Further inclusion of spin-orbit coupling mixes all of these states, leading to thirteen Kramer's

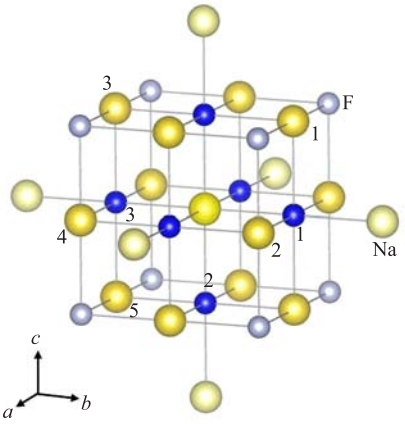

FIG. 1 Coordination environment of Na^+ in the NaF crystal. The numbers on the atoms indicate the symmetrically inequivalent charge-compensating configurations with Ce^{3+} substitution for the central Na^+, namely O_{F1}'-O_{Fi}' (i=2, 3) and V_{Na1}'-V_{Nai}' (i=2−5) in the first and second coordination shells, respectively.

DOI:10.1063/1674-0068/27/05/512-518 ©2014 Chinese Physical Society

TABLE I Lattice constants and volumes of the relaxed NaF (3×3×3) supercells doped with locally charge-compensated Ce^{3+} with site point group symmetries indicated.

		$3a$/Å	$3b$/Å	$3c$/Å	α/(°)	β/(°)	γ/(°)	Volume/Å^3	Volume change[a]
NaF		14.124	14.124	14.124	90.000	90.000	90.000	2817.560	
NaF:Ce^{3+}	O_{F1}'-O_{F2}' (C_{2v})	14.130	14.130	14.133	90.000	90.000	90.012	2821.860	+0.153%
	O_{F1}'-O_{F3}' (D_{4h})	14.140	14.114	14.140	90.000	90.000	90.000	2821.958	+0.156%
	V_{Na1}'-V_{Na2}' (C_s)	14.128	14.120	14.128	89.751	89.977	90.249	2818.189	+0.022%
	V_{Na1}'-V_{Na3}' (C_{2v})	14.131	14.103	14.150	90.000	90.000	90.000	2820.111	+0.091%
	V_{Na1}'-V_{Na4}' (C_2)	14.136	14.116	14.136	89.925	90.002	90.076	2820.976	+0.121%
	V_{Na1}'-V_{Na5}' (D_{2h})	14.122	14.122	14.145	90.000	90.000	90.106	2821.046	+0.124%

[a] The percent changes of volume in last row were calculated with respect to that of the perfect NaF supercell.

doublets that belong to the Γ_2 irreducible representation of the C_1^* double group. In these calculations, a relativistic effective core potential ([Kr] core) with a (14s10p10d8f3g)/[6s5p6d4f1g] Gaussian valence basis set [22] was used for Ce, and an effective core potential ([He] core) with a (5s6p1d)/[2s4p1d] valence basis set [23] was used for F and O. These basis sets were further augmented by the respective auxiliary spin-orbit basis sets for a proper description of the inner core region in the spin-orbit calculations. These wave function-based calculations were performed using the program MOLCAS [24].

III. RESULTS AND DISCUSSION

A. Local structural properties of Ce^{3+}

In perfect NaF lattice (Fm-3m symmetry), the Na^+ ions sit on sites of O_h symmetry, each having six F^- and twelve Na^+ ions in the first and second coordination shells, respectively (Fig.1). The structure of perfect NaF was first optimized with DFT-PBE method, and the calculated value for the lattice constant is 4.708 Å, slightly larger (by ∼1.6%) than the experimental value of 4.634 Å [25], which is due to the intrinsic shortcomings of GGA. The optimized value for the Na−F distance is 2.354 Å, as compared with the experimental value of 2.317 Å. For Ce-doped NaF supercells, the optimized lattice constants are listed in Table I, along with those of perfect NaF for comparison. It can be seen that incorporation of charge-compensated Ce^{3+} into NaF produces very small increases (by 0.09%−0.16%) of the supercell volume and, in some cases, slightly distorts the cubic phase of perfect NaF into phases of lower symmetries, which is especially pronounced for the case with V_{Na1}'-V_{Na2}' compensation. Since the ionic radii of Ce^{3+} and Na^+ in the 6-fold coordination are similar (1.01 and 1.02 Å, respectively) [26], the expansion of the supercell volumes is likely to be caused by the introduction of the charge-compensating O_F' or V_{Na}' defects in the supercells.

In Fig.2, we depict the optimized local structures of charge-compensated Ce^{3+} with the values of selected bond distances indicated and the site point group symmetries identified. Figure 2(a) shows that for the orthorhombic O_{F1}'-O_{F2}' (C_{2v}) center, there is a slight relaxation of Ce^{3+} towards the central position of the two O_F' substituents, due to the larger electrostatic attraction between Ce^{3+} and O^{2-} than that between Ce^{3+} and F^-. The two O_F' move slightly inward, but the other four NN F^- ions remain at their bulk positions. The average distance between Ce^{3+} and the NN anions is 2.355 Å, almost the same as that in perfect system (2.354 Å). For the tetragonal O_{F1}'-O_{F3}' (D_{4h}) center where the two O_F' are on the opposite sides of Ce^{3+} (Fig.2(b)), the position of Ce^{3+} remains unchanged, and the two O_F' move inwards (by 0.207 Å) while the other NN F^- ions move slightly outwards (by 0.067 Å). The average bond length from Ce^{3+} to the NN anions is decreased by 0.024 Å when compared with that in perfect NaF. In the cases of two V_{Na}' vacancies in the second coordination sphere (Fig.2 (c) and (e)), the Ce^{3+} ion relaxes towards the central position of the two V_{Na}', due to the missing electrostatic repulsions with the removed cations. In response to the movement of Ce^{3+} and the presence of V_{Na}' vacancies, the NN anions relax to various degrees, distorting the structure of the coordination shell of Ce^{3+} into lower symmetries. The average Ce−F bond lengths are 2.324, 2.309, and 2.305 Å for V_{Na1}'-V_{Na2}' (C_s), V_{Na1}'-V_{Na3}' (C_{2v}), and V_{Na1}'-V_{Na4}' (C_2) centers, respectively. For the orthorhombic V_{Na1}'-V_{Na5}' (D_{2h}) center (Fig.2(f)), the two vacancies are on the opposite sides of Ce^{3+} and thus the position of Ce^{3+} remains unaltered, but the NN F^- ions still relax due to the absence of the attractions with the vacancies. The average distance from Ce^{3+} to the NN F^- ions is 2.302 Å.

In summary, the occupation of Ce^{3+} at Na^+ site with local charge compensation causes significantly anisotropic distortions of the local structures, which are difficult to predict qualitatively from atomic arrangements of perfect NaF. The quantitative information of these structures are necessary for a reliable calculation of $4f^1$ and $5d^1$ energy levels of Ce^{3+} using a wave function-based embedded cluster method. In ad-

DOI:10.1063/1674-0068/27/05/512-518 ©2014 Chinese Physical Society

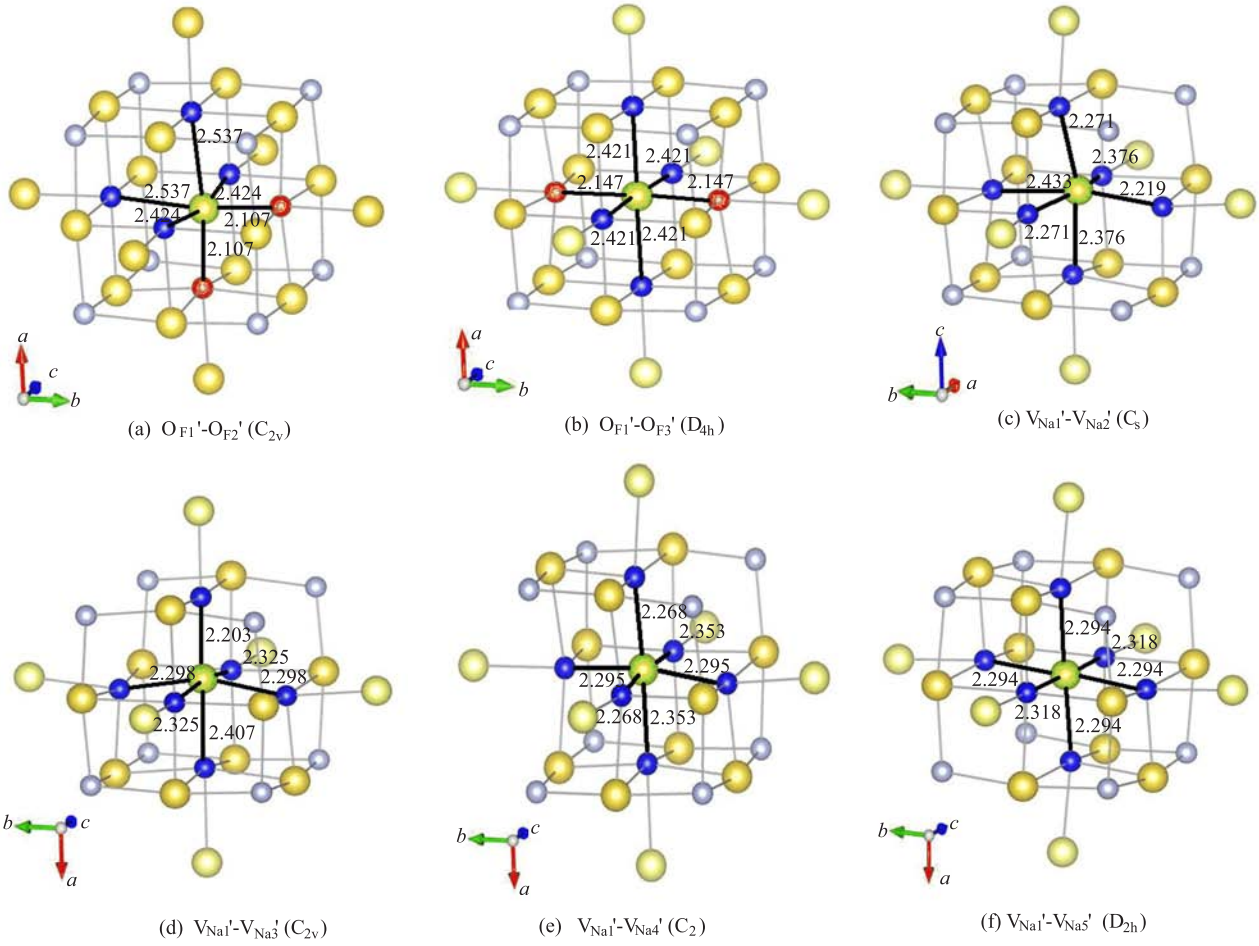

FIG. 2 DFT-optimized local structures of Ce^{3+} in NaF with local charge compensation by two O_F' substitutions or two V_{Na}' vacancies. The central green ball represents the Ce atom, the red balls denote O atoms, and for the other balls the meanings are the same as in Fig.1. The site point group symmetries and the values of selected distances are indicated.

dition, the calculated DFT total energies of the six optimized NaF:Ce^{3+} supercells are listed in Table II. It is seen that the two O_F' compensators in the first coordination shell prefer to be located at neighboring positions (by 173 meV) than at opposite positions. This site preference is consistent with the results from wave function-based embedded cluster calculations (as shown later). When the charge compensation is by two V_{Na}' in the second coordination sphere, the four supercells show comparable stabilities, with the V_{Na1}'-V_{Na3}' configuration slightly more unstable (see Table II).

TABLE II Total energies E_t of Ce-doped NaF supercells calculated with the DFT PBE method.

Ce^{3+} centers	E_t/eV	E_r/meV
O_{F1}'-O_{F2}' (C_{2v})	−943.053691	0
O_{F1}'-O_{F3}' (D_{4h})	−942.881125	173
V_{Na1}'-V_{Na2}' (C_s)	−933.918428	49
V_{Na1}'-V_{Na3}' (C_{2v})	−933.865388	102
V_{Na1}'-V_{Na4}' (C_2)	−933.967149	0
V_{Na1}'-V_{Na5}' (D_{2h})	− 933.928031	39

Note: The relative total energies E_r were calculated with respect to the lowest total energy within each group of charge-compensated centers with O_F' or V_{Na}' compensation, respectively.

B. 4f→5d transitions of charge-compensated Ce^{3+}

From the DFT-optimized structures of NaF:Ce^{3+} supercells with various charge compensations, Ce-centered embedded clusters were constructed with their environments represented by AIMPs and point charges at lattice sites. The wave function-based CASSCF/CASPT2/RASSI SO calculations were then performed to obtain the energies of $4f^1$ and $5d^1$ levels. The results are listed in Table III, from which we see that, in the two cases of O_F' compensation, the lowest $5d_1$ level (at 24546 cm^{-1}) of the orthorhombic C_{2v} center is predicted to be higher by ∼5500 cm^{-1} than that (at 18996 cm^{-1}) of the tetragonal D_{4h} center.

DOI:10.1063/1674-0068/27/05/512-518 ©2014 Chinese Physical Society

TABLE III Calculated $4f^1$ and $5d^1$ energy levels for Ce^{3+} centers in NaF with local charge-compensation by two O_F' or two V_{Na}'. All energies are in unit of cm^{-1}.

	O_{F1}'-O_{Fi}' (i=2, 3)		V_{Na1}'-V_{Nai}' (i=2−5)			
	C_{2v}	D_{4h}	C_s	C_{2v}	C_2	D_{2h}
$4f_1$	0	0	0	0	0	0
$4f_2$	734	728	811	731	778	906
$4f_3$	1205	2092	918	969	1081	1159
$4f_4$	2305	2522	2256	2242	2268	2272
$4f_5$	3081	3515	3001	3020	3143	3148
$4f_6$	3211	4686	3254	3214	3398	3376
$4f_7$	4030	6752	3788	3752	4081	4126
$5d_1$	24546	18996	32986	32200	32468	32161
$5d_2$	27023	32506	35039	33263	33782	33251
$5d_3$	31386	33454	37001	36368	35016	35075
$5d_4$	44636	43455	56596	59181	60894	61022
$5d_5$	58228	51125	58245	60640	61167	62749

By contrast, in the four cases of V_{Na}' compensation, the calculated $5d_1$ level energies are all similar, within the range of 32000−33000 cm^{-1}, but are higher than those of Ce^{3+} with O_F' compensation by an average of ∼10000 cm^{-1}.

From comparison of the calculated and experimental $4f_1 \rightarrow 5d_i$ transition energies, assignments can be made of the experimental excitation bands in association with charge-compensated Ce^{3+} centers (Table III). We first observe that the lowest two weak bands with maxima at 390 nm (25640 cm^{-1}) and 355 nm (28169 cm^{-1}) measured in the excitation spectra can be clearly identified as the $4f_1 \rightarrow 5d_1$, $5d_2$ transitions of the O_{F1}'-O_{F2}' (C_{2v}) center, respectively, with an average deviation of 1100 cm^{-1}. Thus, our calculations provide direct evidence that the observed $4f_1 \rightarrow 5d_1$ transition arises from Ce^{3+} with two O_F' charge compensator in the first coordination shell, rather than from those Ce^{3+} with V_{Na}' compensation as proposed earlier [6, 7]. This result also corroborates the speculation by Dorenbos [4] that the exceptionally large redshift of the $4f_1 \rightarrow 5d_1$ transition in NaF:Ce^{3+} when compared to other Ce^{3+}-doped fluoride compounds is due to the two oxygens on NN fluoride sites. Moreover, these two O_F' compensators are predicted to be located at neighboring positions, and the shape of the coordination polyhedron is deformed to accommodate the O_F' substitutions (Fig.2(a)).

There are also two strong excitation bands at 309 nm (32362 cm^{-1}) and 250 nm (40000 cm^{-1}), which was also observed in absorption spectra of NaF:Ce^{3+} grown in argon. The first band may be ascribed to the first $4f_1 \rightarrow 5d_1$ transitions of the Ce^{3+} centers with V_{Na1}'-V_{Nai}' (i=2−5) compensations in the second coordination sphere (columns 4−7 in Table III). These centers have similar stabilities (as shown by DFT supercell total-energy calculations) and their $4f_1 \rightarrow 5d_1$ transition energies are all in the range of 32000−33000 cm^{-1}. The other band, which is broad with maximum at 250 nm, may be tentatively assigned as the $4f_1 \rightarrow 5d_{2,3}$ transitions of these centers. When the NaF:Ce^{3+} crystals were grown in air, there was a strong band with maximum at 286 nm (34965 cm^{-1}) observed in the absorption spectra. Based on the comparison with the calculated $4f_1 \rightarrow 5d_i$ transition energies of Ce^{3+} with O_F' compensation (columns 1 and 2 in Table III), this band may have contributions from the $4f_1 \rightarrow 5d_{2,3}$ transitions of the O_{F1}'-O_{F3}' (D_{4h}) center.

In Table III, the energies of $4f^1$ and $5d^1$ levels were obtained from wave function-based calculations on Ce-centered embedded clusters constructed from DFT-optimized supercell structures in the ground state. Thus, the calculated $4f_1 \rightarrow 5d_i$ transition energies should be compared to band maxima observed in experimental absorption or excitation spectra. Despite this, we may still make tentative assignments of the three emission bands with maxima at 472 nm (21186 cm^{-1}, band I), 517 nm (19342 cm^{-1}, band II), and 730 nm (13699 cm^{-1}, band III) at room temperature. Bands I and II, which have been ascribed to one type of center on the basis of the luminescence excitation spectra [6], could be assigned as the $5d_1 \rightarrow 4f^1\ ^2F_{5/2}$ and $^2F_{7/2}$ transitions of the O_{F1}'-O_{F2}' (C_{2v}) center assuming a stokes shift of ∼2400 cm^{-1} for the $4f_1 \rightarrow 5d_1$ transition. Similarly, band III could be assigned as the $5d_1 \rightarrow 4f^1\ ^2F_{7/2}$ transition of the O_{F1}'-O_{F3}' (D_{4h}) center.

Based on the above assignments made for 4f→5d transition bands, experimental observations [6, 7] may be interpreted as follows. For the NaF:Ce^{3+} crystal grown in argon, the majority of Ce^{3+} ions reside on Na^+ sites with V_{Na}' compensation, but there are still some Ce^{3+} ions located at Na^+ sites with O_F' compensation due to the presence of oxygen in argon atmosphere. The O_F' compensators with these Ce^{3+} ions are predominant in the O_{F1}'-O_{F2}' (C_{2v}) configuration (Fig.2(a)), since it is energetically preferred over the other O_{F1}'-O_{F3}' (D_{4h}) configuration, as predicted from DFT supercell total energy calculations. The 5d emission bands from Ce^{3+} centers with V_{Na}' compensation were missing in experiments due to the energy transfer to the O_{F1}'−O_{F2}' (C_{2v}) centers. The excitation spectra of the luminescence bands (bands I and II) of the O_{F1}'-O_{F2}' (C_{2v}) centers thus consist of two strong bands ascribed to $4f_1 \rightarrow 5d_{1-3}$ transitions of Ce^{3+} with V_{Na} compensation, and two weak bands assigned to the $4f_1 \rightarrow 5d_{1,2}$ transitions of O_{F1}'-O_{F2}' (C_{2v}) center, respectively. A detailed assignment of the experimentally observed 4f→5d transition bands is presented in Table IV.

C. Effects of O_F' substitutions on the lowest 4f→5d transition energy

The data listed in Table III show that the presence of two neighboring O_F' in the first coordination shell of Ce^{3+} causes a redshift of 7600−8400 cm^{-1} of the

DOI:10.1063/1674-0068/27/05/512-518 ©2014 Chinese Physical Society

TABLE IV Assignments of experimentally observed 4f-5d transition bands in NaF:Ce^{3+}.

	Experimental band[a]/nm	Calculation		
		Center	Transition	Energy/cm^{-1}
4f→5d excitations	390 (25640) (weak)	O'_{F1}-O_{F2}' (C_{2v})	$4f_1 \rightarrow 5d_1$	24546
	355 (28169) (weak)	O_{F1}'-O_{F2}' (C_{2v})	$4f_1 \rightarrow 5d_2$	27023
	309 (32362) (strong)	V_{Na1}'-V_{Nai}' (i=2−5)	$4f_1 \rightarrow 5d_1$	32161−32986
	250 (40000) (strong)	V_{Na1}'-V_{Nai}' (i=2−5)	$4f_1 \rightarrow 5d_{2,3}$	33251−37001
4f→5d absorptions	286 (34965) (strong)	O_{F1}'-O_{F3}' (D_{4h})	$4f_1 \rightarrow 5d_2$	32506
			$4f_1 \rightarrow 5d_3$	33454
5d→4f emissions	472 (21186, band I)	O_{F1}'-O_{F2}' (C_{2v})	$5d_1 \rightarrow (4f^1)^2F_{5/2}$	23900
	517 (19342, band II)	O_{F1}'-O_{F2}' (C_{2v})	$5d_1 \rightarrow (4f^1)^2F_{7/2}$	21390
	730 (13699, band III)	O_{F1}'-O_{F3}' (D_{4h})	$5d_1 \rightarrow (4f^1)^2F_{7/2}$	14630

The bands shown in paratheses are in unit of cm^{-1}.

TABLE V Analysis of energy shift for the lowest $4f_1 \rightarrow 5d_1$ transition from a V_{Na}'-compensated C_{2v} center (A) to a O_F'-compensated C_{2v} center (B) in NaF:Ce^{3+}, in terms of the changes in the centroid-energy difference (ced) and the crystal-field stabilization (cfs) energy. All energies are in unit of cm^{-1}.

		$\Delta E_{ce}(4f^1)$	$\Delta E_{ce}(5d^1)$	$\Delta E_{ced}(4f^1 \rightarrow 5d^1)$	$\Delta E_{cfs}(4f_1)$	$\Delta E_{cfs}(5d_1)$	$\Delta E_{cfs}(4f_1 \rightarrow 5d_1)$	$\Delta E(4f_1 \rightarrow 5d_1)$
$(CeF_6)^{3-}$	A	2167	43482	41315	2167	11713	−9546	31769
$(CeF_4O_2)^{5-}$	B	2081	37164	35083	2081	12618	−10537	24546
	A→B	−86	−6318	−6232	−86	905	−991	−7223

first transition, when compared to those of Ce^{3+} without coordinating O_F' but with two V_{Na}' in the second coordination sphere. In the following, we analyze the electronic reason behind this energy shift. Since this redshift contains two contributions, one from the shift of centroid energy (ce) difference and the other from the change of crystal-field stabilization (cfs) energies, we may decompose the $4f_1 \rightarrow 5d_1$ transition energy into two components [8].

$$\begin{aligned}\Delta E(4f_1 \rightarrow 5d_1) &= [\Delta E_{ce}(5d^1) - \Delta E_{cfs}(5d_1)] - \\ &\quad [\Delta E_{ce}(4f^1) - \Delta E_{cfs}(4f_1)] \\ &= \Delta E_{ced}(4f^1 \rightarrow 5d^1) + \Delta E_{cfs}(4f_1 \rightarrow 5d_1)\end{aligned} \quad (1)$$

where $\Delta E_{ce}(4f^1)$ and $\Delta E_{ce}(5d^1)$ are the centroid energies of $4f^1$ and $5d^1$ configurations relative to the $4f_1$ ground state, and ΔE_{ced} ($4f^1 \rightarrow 5d^1$) is their difference. $\Delta E_{cfs}(4f_1)$ and $\Delta E_{cfs}(5d_1)$ are the energy difference of $4f_1$ and $5d_1$ levels relative to their respective $4f^1$ and $5d^1$ centroid energies. An additional energy-level calculation on an embedded $(CeF_6)^{3-}$ cluster was performed, in which the atomic coordinates and its surrounding are the same as those of the $(CeF_4O_2)^{5-}$ in the O_{F1}'-O_{F2}' (C_{2v}) center, except that two distant Na^+ AIMPs were replaced by vacancies to maintain charge neutrality. As a consequence, the electronic effects of the two O_F' substitution in the O_{F1}'-O_{F2}' (C_{2v}) center on the first $4f_1 \rightarrow 5d_1$ transition energy can be evaluated directly by comparing the results of this additional calculation with those of the O_{F1}'-O_{F2}' center, according to the decomposition scheme described in Eq.(1).

From the last row (A→B) of Table V, we see that the redshift (by 7223 cm^{-1}) of $4f_1 \rightarrow 5d_1$ transition induced by two O_F' substitution in the coordination polyhedron is mainly a consequence of the decrease in the centroid energy difference (−6232 cm^{-1}), which is dominated by the decrease (−6318 cm^{-1}) in the centroid energy of $5d^1$ configuration. Since the geometries of the two coordination polyhedra are the same, this large centroid shift can be explained qualitatively by the much larger polarizability of O^{2-} than F^-, according to the Judd-Morrison model [27, 28]. For the contribution from the crystal-field stabilization energies, the decrease (−991 cm^{-1}) from calculation A to B is caused mostly by the increase (905 cm^{-1}) in that of the $5d_1$ level. This is expected since the stronger interaction between Ce^{3+} and O^{2-} than that between Ce^{3+} and F^- with the same bond distance should lead to a larger crystal-field splitting of $5d^1$ configuration, in view of the delocalization of the Ce^{3+} 5d electron.

IV. CONCLUSION

We have presented a first-principles investigation for the 4f→5d transitions of Ce^{3+} at the Na^+ site in NaF, with local charge compensation by two oxygen substitutions for fluoride (O_F') in the first coordination sphere or by two sodium vacancies (V_{Na}') in the second coordination shell. The DFT-based supercell cal-

DOI:10.1063/1674-0068/27/05/512-518 ©2014 Chinese Physical Society

culations reveal that the incorporation of locally charge-compensated Ce^{3+} induces an anisotropic distortion of the geometry around the dopant site. With the DFT-optimized supercell structures, the Ce-centered embedded clusters were constructed with the embedding environments in NaF simulated by AIMP embedding potentials and point charges at lattice site. The wave function-based CASSCF/CASPT2/RASSI-SO calculations at the spin-orbit level were then performed to obtain the Ce^{3+} $4f^1$ and $5d^1$ energy levels. With the calculated results, we have concluded that the lowest 4f→5d transition, as observed at 390 nm in experimental excitation spectrum, arises from Ce^{3+} with charge compensation by two $O_F{}'$ substitutions at neighboring positions in the coordination polyhedron, rather than by two $V_{Na}{}'$ vacancies as proposed earlier. The experimental 4f→5d transition spectra have also been interpreted in relation to local structures of the dopant Ce^{3+}, in comparison with the theoretical results. Finally, we analyzed the electronic reason for the large redshift (by $\sim$8000 cm^{-1}) of the lowest 4f→5d transition as induced by two neighboring $O_F{}'$ substitutions in the coordination polyhedron, from two independent aspects of centroid shift and crystal-field splitting. The present study demonstrates the ability of *ab initio* methods in elucidating the spectral properties of Ce^{3+} with complex environments usually observed in Ce-doped luminescent materials.

V. ACKNOWLEDGMENTS

This work was supported by the National Natural Science Foundation of China (No.11174005).

[1] P. Lecoq, A. Annenkov, A. Gektin, M. Korzhik, and C. Pedrini, *Inorganic Scintillators for Detector Systems: Physical Principles and Crystal Engineering*, Heidelberg: Springer-Verlag, (2006).
[2] W. M. Yen, A. Shionoya, and H. Yamamoto, *Phosphor Handbook*, 2nd Edn., Boca Raton: CRC Press, (2007).
[3] A. A. Kaminskii, Laser Photon. Rev. **1**, 93 (2007).
[4] (a) P. Dorenbos, Phys. Rev. B **62**, 15640 (2000).
(b) P. Dorenbos, Phys. Rev. B **62**, 15650 (2000).
(c) P. Dorenbos, Phys. Rev. B **64**, 125117 (2001).
[5] P. Dorenbos, J. Lumin. **91**, 91 (2000).
[6] V. F. Pisarenko, G. D. Potapenko, and V. V. Popov, Opt. Spectrosc. **38**, 51 (1975).
[7] V. F. Pisarenko, G. D. Potapenko, and V. V. Popov, Opt. Spectrosc. **39**, 522 (1975).
[8] A. B. Muñoz-García, J. L. Pascual, Z. Barandiarán, and L. Seijo, Phys. Rev. B **82**, 064114 (2010).
[9] L. Ning, L. Lin, L. Li, C. Wu, C. Duan, Y. Zhang, and L. Seijo, J. Mater. Chem. **22**, 13723 (2012).
[10] J. Wen, L. Ning, C. Duan, Y. Chen, Y. Zhang, and M. Yin, J. Phys. Chem. C **116**, 20513 (2012).
[11] B. K. Dzholdoshov, M. M. Kidibaev, T. S. Koroleva, A. N. Cherepanov, D. V. Raĭkov, V. Yu. Ivanov, and O. V. Ryabukhin, Phys. Solid State **47**, 1470 (2005).
[12] B. V. Shulgin, A. N. Tcherepanov, V. Yu Ivanov, T. S. Koroleva, M. M. Kidibaev, C. Pedrini, and C. Dujardin, J. Lumin. **125**, 259 (2007).
[13] J. P. Perdew, K. Burke, and M. Ernzerhof, Phys. Rev. Lett. **77**, 3865 (1996).
[14] J. P. Perdew, K. Burke, and M. Ernzerhof, Phys. Rev. Lett. **78**, 1396 (1997).
[15] G. Kresse and J. Furthmüller, Phys. Rev. B **54**, 11169 (1996).
[16] G. Kresse and D. Joubert, Phys. Rev. B **59**, 1758 (1999).
[17] P. E. Blöchl, Phys. Rev. B **50**, 17953 (1994).
[18] L. Seijo, http://www.uam.es/quimica/aimp/Data/AIMP Libs.html
[19] J. Gracia, L. Seijo, Z. Barandiarán, D. Curulla, H. Niemansverdriet, and W. van Gennip, J. Lumin. **128**, 1248 (2008).
[20] A. Gellé and M. Lepetit, J. Chem. Phys. **128**, 244716 (2008).
[21] P. Å. Malmqvist, B. O. Roos, and B. Schimmelpfennig, Chem. Phys. Lett. **357**, 230 (2002).
[22] L. Seijo, Z. Barandiarán, and B. Ordejón, Mol. Phys. **101**, 73 (2003).
[23] Z. Barandiaran and L. Seijo, Can. J. Chem. **70**, 409 (1992).
[24] G. Karlström, R. Lindh, P. Å. Malmqvist, B. O. Roos, U. Ryde, V. Veryazov, P. O. Widmark, M. Cossi, B. Schimmelpfennig, P. Neogrady, and L. Seijo, Comput. Mater. Sci. **28**, 222 (2003).
[25] M. P. Tosi, Solid State Phys. **16**, 1 (1964).
[26] R. D. Shannon, Acta Cryst. A **32**, 751 (1976).
[27] B. R. Judd, Phys. Rev. Lett. **39**, 242 (1977).
[28] C. A. Morrison, J. Chem. Phys. **72**, 1001 (1980).

DOI:10.1063/1674-0068/27/05/512-518 ©2014 Chinese Physical Society